

RESEARCH ARTICLE

X-Ray Diffraction Analysis of Sigma-Phase Evolution in Equimolar AlCoCrFeNi High Entropy Alloy

Mudassar Hussain¹, Abdilllah Sani Mohd Najib^{1,2}, Nor Akmal Fadil^{1,2}, Tuty Asma Abu Bakar^{1,2*}

¹Department of Materials, Manufacturing & Industrial Engineering, Faculty of Mechanical Engineering, Universiti Teknologi Malaysia, 81310 Johor Bahru, Johor, Malaysia

²Materials Research and Consultancy Group, Faculty of Mechanical Engineering, Universiti Teknologi Malaysia, 81310 Johor Bahru, Johor, Malaysia

ABSTRACT – Novel equimolar AlCoCrFeNi high entropy alloy (HEA), as a promising candidate for demanding engineering applications has recently received considerable attention due to its random solid solution structure. It confers its synergy of high strength, ductility, high-temperature structure stability and corrosion resistance. Thermally assisted spinodal dissolution from BCC random solid solution (B1) to ordered BCC (B2) and precipitation of brittle σ -phase renders its ability to undergo as an alloy for thermomechanical processing. Therefore, it was necessary to manifest σ -phase nucleation and growth from homogenization temperature (1250°C) at different cooling rates, i.e., furnace cooled and water quenched along with variation in σ -phase crystallite size at transformation temperature (800°C) in Fibonacci time frame (1h, 2h, 4h, 8h, and 16h) to know hot working temperature range and post treatment. An equimolar AlCoCrFeNi high-entropy alloy fabricated via vacuum induction melting was subjected to ICP-MS and XRD analysis to confirm its chemical composition and crystal structure distribution. The XRD results were further analyzed by using Scherrer's equation and Williamson-Hall plot to calculate the crystallite size of σ -phase and its associated microstrain. The work aimed to determine the σ -phase reversibility from homogenization temperature 1250°C and crystallite size growth at transformation temperature (800°C) to reveal the importance of thermomechanical processing parameters of equimolar AlCoCrFeNi HEA. In the present study, remarkable retention of the FCC phase was witnessed during furnace cooling and its traces appeared during rapid cooling. The vital phenomenon of FCC-phase nucleation signifies the key importance of the transformation zone, revealing its effect on the post-treatment cooling rate. However, its coupled phenomenon of the tetragonal σ -phase formation remained suppressed during cooling from homogenization temperature (1250°C). It determined the wide hot workability range of equimolar AlCoCrFeNi HEA to make it a suitable candidate for bulk engineering applications.

ARTICLE HISTORY

Received : 13th July 2024

Revised : 17th Nov. 2024

Accepted : 12th Dec. 2024

Published : 19th Dec. 2024

KEYWORDS

Equimolar AlCoCrFeNi High entropy alloy (HEA)

σ -phase

Crystallite size

Micro strain

X-ray diffraction

1. INTRODUCTION

Metallic materials account for a sizable share of engineering applications. The conventional alloy design includes one element as a foundation of alloy and the rest of the elements as major and minor alloying additions, with a few microalloyings and modifiers employed as specialized property enhancers [1]. The conventional alloy systems that contain a principal component are shaded with a new concept of multi-principal elemental alloys named high entropy alloys (HEA) from the last one and half decades. High entropy alloys are multi-principal element alloys that contain at least five elements with a target composition of 5 % ~ 35 % at each, whereas the minor elements should be less than 5 % [2]. However, concurrent reporting of multi-principal element alloys or high entropy alloys by Cantor, Chang et al. (2004), and Yeh et al. (2004) triggered a new approach to designing metallic alloys. Lately, it has not only been limited to metals and their alloys but also extended to ceramics, polymers and other classes of materials [3, 4]. In the case of crystal structure diversity, these alloys may be FCC, BCC, HCP, duplex or triplex. Still, classification against physical properties is generally reported based on low-density, refractory and eutectic high entropy alloys.

Considering the detailed nature of elemental construction, high-entropy alloys can be classified into five subclasses. Transition metal high-entropy alloys (THEA) mostly exhibit an FCC crystal structure. Refractory metal high-entropy alloys (RHEA) are dominated by BCC, L12, B2, HCP, and Laves phases (C14 and C15). Low-density high-entropy alloys (LDHEA) typically show HCP structures, while high-entropy alloys containing at least four lanthanides predominantly exhibit an HCP phase. Another subclass, known as oxide dispersion-strengthened high-entropy alloys (ODSHEA), incorporates any of the aforementioned classes as a matrix combined with nano-oxide dispersions [5]. These dispersions synergistically enhance high-temperature strength and corrosion resistance. Synergistic properties of high strength, ductility, temperature stability, fracture toughness and corrosion resistance outclass AlCoCrFeNi's high entropy alloy system for robust engineering applications [6]. Due to its adaptability in microstructure and phase tailoring with various alloying compositions from single-phase (BCC) to duplex (BCC + FCC) and triplex (BCC + FCC + IM) alloys,

AlCoCrFeNi alloy puts itself in primarily explored high entropy alloy systems [7]. However, when these alloys display eutectic phase morphology, another feature comes into play.

Literature studies suggested that the synthesis route of a high entropy alloy system greatly influences the phase formations and crystal structure. Mostly, standard casting routes are reported on single-phase BCC structures in equimolar AlCoCrFeNi high entropy alloy (HEA) [8]. However, production via mechanical alloying and ball milling dual phase (FCC and BCC) will likely occur. According to Wang et al. (2021), vacuum arc melting produced high entropy AlCoCrFeNi alloys with single-phase BCC crystal structures. However, many reports on alloy production by using powder metallurgy or casting predicted the creation of additional phases following consolidation [9]. Mohanty et al. (2017) explored the phase development in AlCoCrFeNi high entropy alloys produced by mechanical alloying and subsequent sintering. The study reported on the emergence of a tetragonal σ -phase which contained Cr-Fe-Co, while Al-Ni rich L12 ordered γ' phase and Al-Ni-Co-Fe FCC solid solution phase as a matrix for sample sintered from 699.85°C to 999.85°C [10]. Ji et al. (2014) reported that the AlCoCrFeNi high entropy alloy had a two-phase microstructure with BCC and FCC phases. It was produced by mechanical alloying and consolidation under spark plasma sintering at 900°C [11].

While reviewing heat treatment temperature and time impact on phase transformation of equimolar AlCoCrFeNi HEA after initial consolidation via conventional casting or powder metallurgy route, a previous study showed that the σ -phase was frequently generated in the inter-dendritic (ID) region governed by diffusional transformation of BCC to FCC, solute rejection of Fe and Cr, which lowered the toughness of alloy, plasticity and corrosion resistance. However, it also narrated that the σ -phase changed to the BCC/B2-phase at high temperatures. For instance, Strumza et al. (2022) discovered that the σ -phase would transmute into BCC/B2 particles at 960.1°C. The formation of σ -phases in the AlCoCrFeNi HEA system reduced its potential for further hot rolling, forging and extrusion. The mechanisms of σ -phase evolution and genesis have yet to be extensively explored and described. To improve the "strength-ductility trade-off," managing the phase transition of the σ - phase and FCC phase is necessary [12]. The quench sensitivity of any alloy determines its applicability, range of achievable mechanical properties and selection of thermomechanical processing (TMP) parameters and equipment. Like conventional alloys (steels, titanium alloys and aluminum alloys), prospects of equimolar AlCoCrFeNi HEA are required to determine, in this regard, time-temperature-transformation (TTT) curves are important in determining phase precipitation during TMP and cooling [13-15]. Comprehending the σ -phase nucleation and growth during steady-state development at exposed temperatures over different periods is crucial.

An X-ray diffraction (XRD) analysis of polycrystalline materials reveals clear peaks that correlate to various reflection planes, confirming the crystalline nature of the sample. The observed widening of XRD peaks was caused by a combination of lattice strain and crystallite size with size restriction, resulting in intrinsic lattice strain. In addition to the widening caused by differences in size, lattice strain may also be induced by many variables, such as stacking faults, grain boundary junctions, point defects, dislocation density, and stress. Therefore, examining XRD peak broadening is useful for understanding the inherent strain and dimensions of nanoparticles, which can subsequently impact material characteristics. Elastic characteristics may also be obtained from this inherent strain, such as energy density and strain. Various approaches, including Rietveld refinement, Balzar method, Warren-Averbach analysis, Fourier techniques and Williamson-Hall analysis can be used to calculate the contributions of crystallite size and lattice strain to peak broadening. Although the Warren-Averbach and Balzar techniques consider size and strain broadening, they are incompatible with Stokes-Fourier de-convolution methodology [16, 17]. On the other hand, the Williamson-Hall approach uses full width at half maximum (FWHM) of the diffraction peak to calculate characteristics like average size, strain, stress, Young's modulus and energy density.

Substantial work was reported on water quenching to freeze the microstructure from higher temperatures for onward characterization and, to some extent, for normalizing. However, the practical cooling rate falls between normalizing and furnace cooling during TMP, like rolling and forging. The gap lies in the lack of understanding of the sigma phase coarsening during exposure and staying in the transformation range during thermomechanical processing or preheating and its re-nucleation while cooling from hot working or homogenization temperature. In this work, the focus was on determining the kinematics of phase transformation during heating and cooling, explicitly the σ -phase in vacuum induction melted equimolar AlCoCrFeNi HEA at a transformation temperature of 800°C for Fibonacci time frame (1h, 2h, 4h, 8h, and 16h) and influence of cooling rate from high-temperature single-phase homogenization on σ -phase reoccurrence.

2. METHODS AND MATERIAL

2.1 Material Design and Its Fabrication

Before preparing the equimolar AlCoCrFeNi HEA, a systematic material design approach was adopted from the empirical parameters calculation reported for predicting phase stability of high entropy alloys with MATLAB-based software (HEAPS) and then further verified by the already reported CALPHAD results [18, 19]. Experimental results further verified these simulated results and an equimolar high entropy alloy AlCoCrFeNi was prepared by using 99.99 pure elements of Al, Co, Cr, Fe and Ni in a vacuum induction furnace (VIM) as induction melting tends to homogenize the chemical composition of the melt due to its natural stirring instinct. A high vacuum of 10^{-5} mbar was initially maintained during melting and casting. Then, high-purity Ar gas was purged in the chamber to maintain an atmospheric

pressure of 500 mbar ~ 800 mbar to reduce elemental losses. Induction melting was used to agitate the melting process and guarantee the chemical homogeneity of a highly concentrated chemical composition. The melting and casting process was done three times to ensure a chemically uniform melt and prevent segregation. The molten AlCoCrFeNi was poured into a ceramic mould to solidify. The slow cooling was adopted to ensure spinodal decomposition occurs as it was specifically associated with AlCoCrFeNi high-entropy alloy.

2.2 Composition Analysis

The quantitative elemental composition of cast ingot was determined by employing PerkinElmer Avio 200 ICP-OES to ensure that comparison with the amounts of individual elements was added. The high-entropy alloy samples were precisely measured to a specific mass by using an analytical balance. Subsequently, the samples were dissolved in a solution of strong nitric acid (HNO₃) and hydrochloric acid (HCl) in a 3:1 ratio, often aqua regia. The dissolving procedure was performed by using a microwave digesting machine to guarantee full disintegration. The resultant solution was diluted to a predetermined volume by using deionized water. The samples in solution were passed through a membrane filter to exclude any solid particles that were not dissolved, thereby guaranteeing a transparent solution suitable for analysis. The calibration standards were created using high-purity solutions that contained just a single ingredient.

To prepare a set of standards included the dilution of the stock solutions with deionized water to achieve the desired concentration range of analytes in samples. A standard solution was internally generated and added to the calibration standards and sample solutions to compensate for any fluctuations in instrument conditions. The ICP-OES instrument was set up by following the manufacturer's instructions. The torch, nebulizer and spray chamber were installed and properly aligned. The plasma was ignited, and the device was allowed to reach a stable temperature and state for a certain duration, as instructed by the manufacturer. The instrument parameters, such as nebulizer gas flow, auxiliary gas flow, RF power and sample absorption rate, were fine-tuned to attain optimal sensitivity and accuracy.

The wavelengths for each element were carefully chosen to minimize any spectral interferences and a background correction was included to account for any matrix effects. Calibration standards were implemented into the ICP-OES instrument, and their emission intensities were monitored to generate calibration curves for each element. Sample solutions were subsequently presented, and their emission intensities were documented. Calibration curves were generated by plotting emission intensities of the calibration standards against their known corresponding concentrations. Quality control samples such as certified reference materials (CRMs) were examined along with the samples to confirm the correctness and precision of measurements. Additional analyses were conducted to verify the consistency of the findings. Concentrations of components in sample solutions were determined by using these calibration curves. The amounts of each element in the high-entropy alloy samples were determined and expressed in suitable measures, such as weight percent (wt%) or parts per million (ppm).

2.3 Heat Treatment

The phase fraction simulation of equimolar AlCoCrFeNi HEA was considered a reference to evaluate the phase evolution over the temperature range for heat treatment. The analyzed chemical composition was used to calculate high-entropy alloy empirical factors to verify the concerned phase stability. Now, there were two areas of concern: one was related to sigma-phase growth, while the second was related to reversibility or recurrence of the sigma-phase during cooling from the BCC single-phase. A comprehensive heat treatment was carried out based on previous findings by various researchers to determine the σ -phase kinematics over the period at phase transformation temperature, as shown in Figure 1.

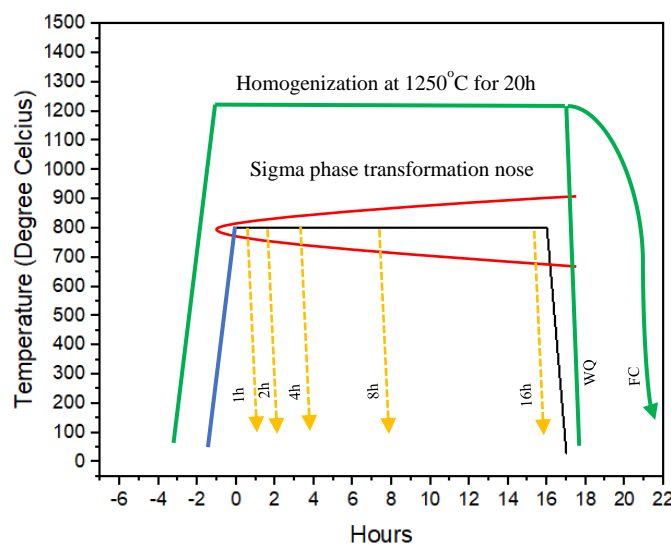


Figure 1. Heat treatment cycle for equimolar AlCoCrFeNi HEA

The selection of transformation temperature (800°C) was made based on the temperature range in which the σ -phase existed as reported. The Fibonacci time frame was adopted (1h, 2h, 4h, 8h and 16h to reduce the number of samples for evaluation of the σ -phase in AlCoCrFeNi HEA without compromising the accuracy of results for the specific time range. However, to confer the recurrence of the σ -phase during cooling from homogenization temperature (1250°C), water quenching (WQ) and furnace cooling (FC) were adopted.

2.4 X-Ray Diffraction and Crystal Structure Analysis

One effective method to identify different crystalline material structural characteristics is X-ray diffraction (XRD). The XRD analysis was conducted by using Rigaku Smart Lab (45KV-200mA) with Cu- α radiation ($\lambda=1.5406\text{nm}$) at a scanning rate of $3^\circ/\text{min}$ and step size 0.2° between 20° to 100° to determine the phase constituents and their evolution over the temperature range and exposure time in cast and heat-treated equimolar AlCoCrFeNi HEA. A slower scanning rate than usual was adopted to ensure that reflections from low-concentration phases were obtained. The raw XRD pattern of each sample was processed to remove its background noise and smooth it for onward processing to Rietveld Refinement, peak matching and determining the full-width half maximum (FWHM) of corresponding peaks. After cleaning and processing XRD data, Scherrer equation and Williamsons-Hall plot (W-H plot) method were adopted to calculate the crystallite size of the rich tetragonal σ -phase and its corresponding microstrain in each sample.

3. RESULTS AND DISCUSSION

ICP-OES was used to verify the equimolar composition of AlCoCrFeNi high entropy alloy. Its results suggested a composition drift from ideal equimolar composition because iron (Fe) content was the highest while aluminum (Al) was on the lowest side of the compositional range. However, its nearly equimolar composition was still validated.

Table 1. Chemical composition of equimolar AlCoCrFeNi high entropy alloy

Sr. No.	Element	Composition at %
1	Al	17.46 \pm 0.018
2	Co	19.61 \pm 0.019
3	Cr	19.86 \pm 0.020
4	Fe	21.97 \pm 0.022
5	Ni	21.09 \pm 0.021

Empirical factors that predict the stability of the solid solution phase, probable crystal structure and occurrence of intermetallics were widely used criteria. These factors and criteria helped to predict feasible molar combinations of elements and their types for synthesizing high-entropy alloys. The concise MATLAB tool with GUI was recently developed under high entropy alloy predicting software (HEAPS) [18]. It is used to predict the stability of the solid solution, crystal structure, presence of intermetallics and mechanical behavior of equimolar AlCoCrFeNi HEA. While calculating these empirical factors by using HEAPS, it could be concluded diversity in the prediction of microstructure criteria (MC1-10) with the results of solid solution (SS), intermetallics (IM), multiple solid solutions (MPSS) and their combination as well. Such diversity lies in a limited batch of alloys taken to devise each criterion. According to criteria MC3, it is not certain whether the alloy containing this equimolar composition will be crystalline or amorphous. Meanwhile, MC6 and MC8 predicted the stability of multiple solid solutions instead of a single solid solution. However, MC5, MC7, MC9 and MC10 predicted the stability of the intermetallic phase as bulk instead of supporting the stability of the solid-solution phase.

These four criteria are near the conventional understanding of mixing multiple elements in equimolar concentrations. Therefore, it is based on the dominant enthalpy factor of mixing instead of the entropy of mixing. Similarly, lattice structure stability (LSS1-5) criteria predict only BCC and BCC+FCC. Here, LSS1 and LSS 3 predicted that the major stable phases will be BCC and FCC together, containing a duplex structure, while LSS 2 supports the stability of the BCC phase. However, LSS 4 and LSS 5 were uncertain about confirming any crystal structure combinations. However, LSS 2 predicted the stability of single-phase structures that contained BCC crystals instead. The intermetallics phase predictor (ImF3) confirmed laves-free microstructure, while ImF1 and ImF 2 were uncertain about predicting the presence of TCP and σ -phase in the final microstructure. The mechanical behavior that predicts criteria FMP1 confirms the brittle behavior of equimolar AlCoCrFeNi high-entropy alloy. These criteria have limitations in using the data related to specific high-entropy alloy systems and are sometimes limited to certain processing and synthesis methods. Therefore, their predictions are contemporary and not highly accurate. Still, they give insight into starting the research work for specific alloy systems and mole fractions instead of going blindly with the hit-and-trial method. To further validate, it could be referred to as CALPHAD simulation results.

Table 2. Empirical calculation results for equimolar AlCoCrFeNi HEA

Parameters	Symbol	Values	Criteria	Status
Melting Temperature of Alloy	T _m (K)	1684	MC1 $\Delta H^m - \delta r$	SS
Avg. atomic weight	At. Weight (g·mol ⁻¹)	50.49	MC2 $\Omega - \delta r$	SS
Density	ρ (g·cm ⁻³)	7.10	MC3 $\delta r - \Delta H^m$	Uncertain
Heat Capacity	C _p (J·mol ⁻¹ ·K ⁻¹)	24.71	MC4 γ	SS
Thermal Conductivity	The (W·m ⁻¹ ·K ⁻¹)	120.32	MC5 $\delta \chi^A - \delta r$	IM
Atomic radii	r (pm)	128.38	MC6 Λ	MPSS
Paulling's Electronegativity	χ^p (-)	1.78	MC7 T/T _m - $\delta r - \Delta H^m$	IM(0.5 < T/T _m < 0.9)
Allen's Electronegativity	χ^A (-)	1.76	MC8 ϕ	MPSS/IM
Valance Electron Concentration	VEC (-)	7.20	MC9 $\eta - \Delta H^{ic}$	IM
Atomic Size Difference	e/a (-)	2	MC10 Δk	IM
Percentage change in r	δr (%)	5.77	LSS1 VEC	BCC+FCC
Percentage change in χ^p	$\delta \chi^p$ (%)	6.781	LSS2 VEC-e/a	BCC
Change in Paulling's Electronegativity	$\Delta \chi^p$ (-)	0.121	LSS3 T/T _m -VEC	BCC+FCC(0.5 < T/T _m < 0.9)
Percentage change in χ^A	$\delta \chi^A$ (%)	6.076	LSS4 ϕ -VEC	Uncertain
Change in Allen's Electronegativity	$\Delta \chi^A$ (-)	0.107	LSS5 T-VEC-r- $\Delta \chi^A$ - ΔVEC	Uncertain
Change in Valance Electron Concentration	ΔVEC (-)	2.48	ImF1 $\Delta \chi^p$	Uncertain
Change in Mixing Enthalpy	ΔH^m (kJ·mol ⁻¹)	-12.32	ImF2 PSFE-VEC	Uncertain
Change in Mixing Entropy	ΔS^m (J·mol ⁻¹ ·K ⁻¹)	13.38	ImF3 $\delta \chi^A - \delta r$	Laves Free
Change in Gibbs Free Energy	ΔG^m (kJ·mol ⁻¹)	-25.70	FMP1 VEC	Brittle
Change in	ΔH^{ic} (kJ·mol ⁻¹)	-66.10		
S ^{ss} (bcc) (J·mol ⁻¹ ·K ⁻¹)	S ^{ss} (bcc) (J·mol ⁻¹ ·K ⁻¹)	-0.76853		
S ^{ss} (fcc) (J·mol ⁻¹ ·K ⁻¹)	S ^{ss} (fcc) (J·mol ⁻¹ ·K ⁻¹)	-1.2434		
Gama Factor	γ (-)	1.1691		
Omega Factor	Ω (-)	1.83		
Λ Factor	Λ (J·mol ⁻¹ ·K ⁻¹)	0.402		
ϕ (bcc) Factor	ϕ (bcc) (-)	7.893		
ϕ (fcc) Factor	ϕ (fcc) (-)	4.878		
η Factor	η (-)	0.077		
$\Delta \kappa$ Factor	$\Delta \kappa$ (-)	-3.94		
Stacking Fault Energy	PSFE (%)	40		

The phase fraction simulation is a reference from earlier research calculated by using Thermo-Calc software with TCHEA2 [19]. This simulation confirms multiple solid solutions phase morphologies, which contain BCC-phase and B2-phase at room temperature (Figure 2). Co-Fe-rich BCC-phase and Cr-rich BCC-phase annihilated to transform into Cr-rich σ -phase and partly to NiAl B2 phase as its phase fraction also increased between temperature range of 400°C to 600°C. At 600°C a new Co-Cr-Fe rich FCC-phase was nucleated and grew up to 1000°C. The Cr rich σ -phase disappeared at 900°C, and another Cr-Fe rich BCC-phase appeared at this temperature. The BCC-phase fraction increased to 0.7 mole fraction. However, the Ni-Al B2-phase started to melt at around 1300°C. It could be seen that the rich σ -phase originated at the expense of disordered BCC structures. However, at the later stages of its growth, Co-Cr-Fe rich FCC nucleated and rowed at the expense of Co-Fe rich BCC-phase and Cr rich σ -phase. XRD patterns in Figure 3 were captured from solid samples in as-cast condition and at 800°C for 1, 2, 4, 8, and 16 h at a scanning rate of 3°/min to determine the phases and crystal structure evolved during the heat treatment process. Two as-cast samples were homogenized at 1250°C for 20 h. This step followed the first water quenching and the second furnace cooling before XRD analysis. It was to determine the recurrence of certain phases with changing cooling rates and know the quench sensitivity.

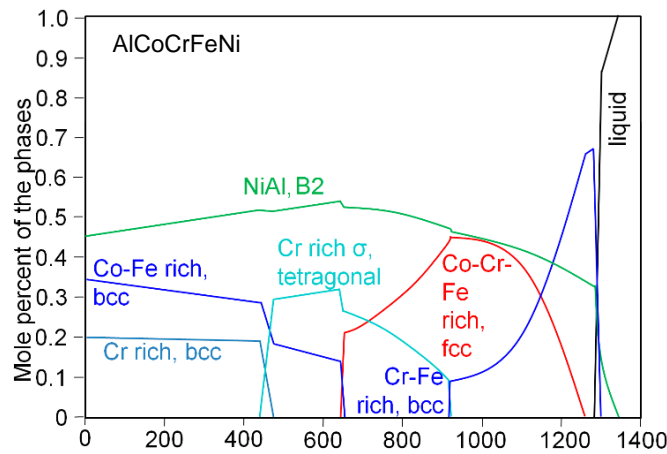


Figure 2. Phase fraction simulation of equimolar AlCoCrFeNi HEA by CALPHAD method

The cast sample exhibited a duplex crystal structure that contained B2/BCC and FCC crystal structures, which agreed with the results reported earlier via the same manufacturing method but was contrary to those of a few researchers. Peaks that corresponded to 2θ values of 43.6 and 50.8° suggested the FCC/L12 Cr-Fe-Ni rich phase (PDF#33-0397), while 44.06, 64.26, and 90.77° corresponded to the presence of the B2/BCC-phase [15]. X-ray diffraction pattern of heat-treated samples at 800°C for 1h altered the morphology of the diffraction pattern in comparison with the cast sample. New relatively low-intensity peaks at 42.443°, 43.848°, 44.949°, 46.183°, 47.097°, and 48.457° appeared, representing the tetragonal Cr-Fe σ -phase (PDF#05-0708) and other peaks confirming FCC and B2/BCC phases [20]. No new diffraction peak appeared while increasing the holding time at 800 °C until 2h. However, peak intensity changed at 4h and 8h, suggesting the alteration of phase fractions, and new low-angle peaks at 30.9° and 35.3° appeared, reinforcing the precipitation of Al-Ni intermetallics [21, 22]. Strong FCC corresponding peaks suggested diffusion-assisted phase transformation occurred at the expense of BCC/B2-phase, resulting in the Cr-Fe depleted FCC phase and Cr-Fe rich BCC and tetragonal σ -phase. Exposure at 800°C for 16h did not affect the number of phases present. However, peak intensity changed noticeably.

The XRD pattern of the sample exposed to 1250°C for 20h and then water quenched showed a remarkable difference in diffraction peaks. Low-intensity diffraction peaks at 42.443°, 43.848°, 44.949°, 46.183°, 47.097°, and 48.457° disappeared, suggesting that the tetragonal σ -phase dissolved to BCC/FCCL12-phases. The XRD pattern of the furnace-cooled sample from 1250°C followed a relatively different pattern with the disappearance of L12-phase corresponding peaks, suggesting the rearrangement of Al-Ni-phases.

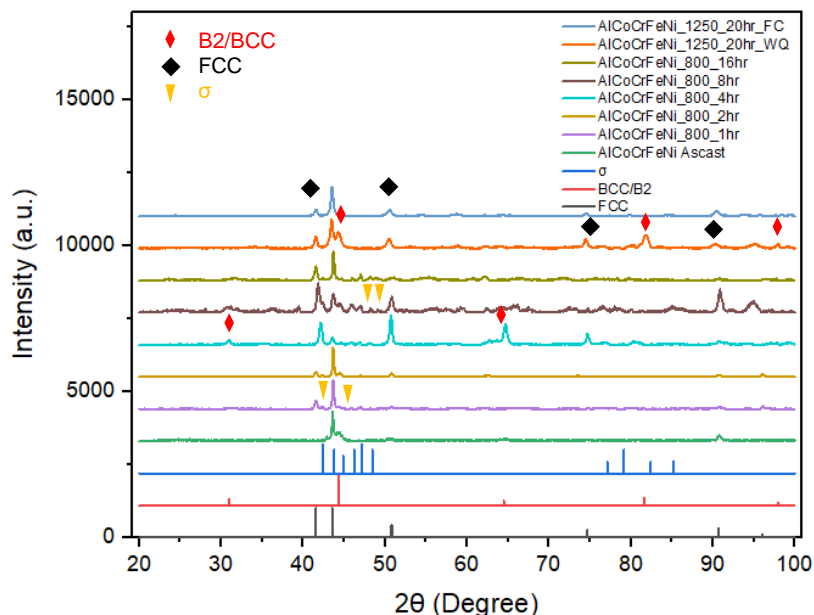


Figure 3. XRD patterns in As-cast and heat-treated conditions

Microstrain, crystallite size, and growth are important factors to consider when analyzing XRD data to comprehend the microstructure and mechanical characteristics of the material. The size of a coherent, crystalline area inside a material is referred to as crystallite size. Given that a grain might comprise several smaller crystallites, the grain size is not always the same.

The Scherrer equation, which connects the size of crystallites to the broadening of X-ray diffraction peaks and does not include the impact of strain on peak broadening, may be used to determine the size of crystallites. However, the total X-ray diffraction peak broadening results from size and strain.

$$D = \frac{K\lambda}{\beta \cos\theta} \tag{1}$$

where:

D = Size of crystallite

K is the Scherrer constant, which, depending on the crystallite's form, is normally about 0.9.

λ represents the X-ray's wavelength.

β represents the diffraction peak's full width at half maximum (FWHM) in radians.

θ is the Bragg angle or the angle where the peak appears.

The XRD pattern widening of peaks can be used to determine the average crystallite size. When stresses within crystallites arise from lattice distortions, it is referred to as microstrain. Extra widening of the XRD peaks is caused by these stresses. The analysis of XRD peak broadening in combination with crystallite size can be used to quantify microstrain. This is frequently accomplished by using the Williamson-Hall plot. The equation known as Williamson-Hall is as follows:

$$\beta \cos\theta = 4\epsilon \sin\theta + K\lambda D \tag{2}$$

where,

$\beta \cos\theta$ = Broadening contribution due to the size of the crystallite

$4\epsilon \sin\theta$ = Microstrain-related broadening contribution

The Williamsons-Hall plot (W-H plot) derived from the XRD pattern of corresponding samples (Figure 4) in as-cast and heat-treated conditions indicated a change in slope from positive to negative value. In the W-H plot, the slope value equals the microstrain of a particular phase under which it exists [23]. While determining the microstrain and y-intercept values via the W-H plot, only peaks related to the tetragonal σ -phase in the sample heated for 1 h at 800°C exhibited a positive value of the slope, indicating the positive microstrain value.

The intercept and slope of the linear fit were used to independently calculate the crystallite size and microstrain by displaying $\beta \cos\theta$ against $4\sin\theta$. XRD results were further used to calculate the variation in microstrain and crystallite size of the tetragonal σ -phase over time using the Scherrer equation and Williamson-Hall (W-H) plot. Microstrains and crystallite size greatly influence multiple properties of alloys like small crystallite sizes improve mechanical properties by increasing sub-grain structure, while larger crystallite sizes are more stable at increased temperatures. On the other hand, higher microstrains in crystal structure are negatively influenced by promoting stress corrosion cracking, fatigue crack initiation, and localized stress-induced transformations [24-27].

However, the slope changed from positive to negative by increasing the holding time in the Fibonacci time frame (1h, 2h, 4h, 8h, and 16 h). It concluded that the tetragonal σ -phase had a negative microstrain, identifying it under compression. The crystallite size of the tetragonal σ -phase tended to vary from 3.12nm to 68.37 nm with a -gradual increase from 8h to 16 h after exposure at 800°C (Figure 5).

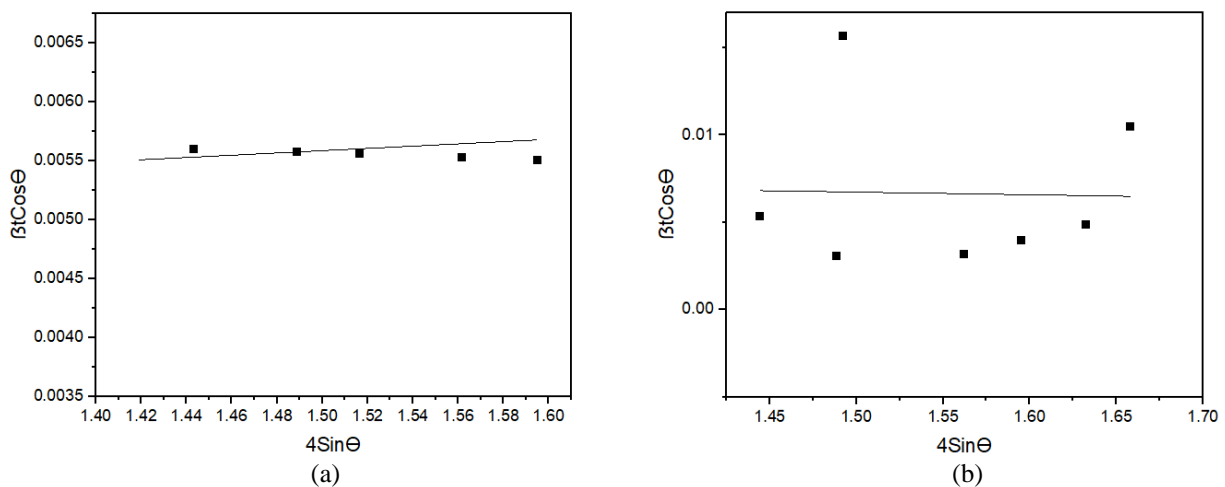


Figure 4. Williamson-hall plot (a) As cast; (b) 1hr @800°C

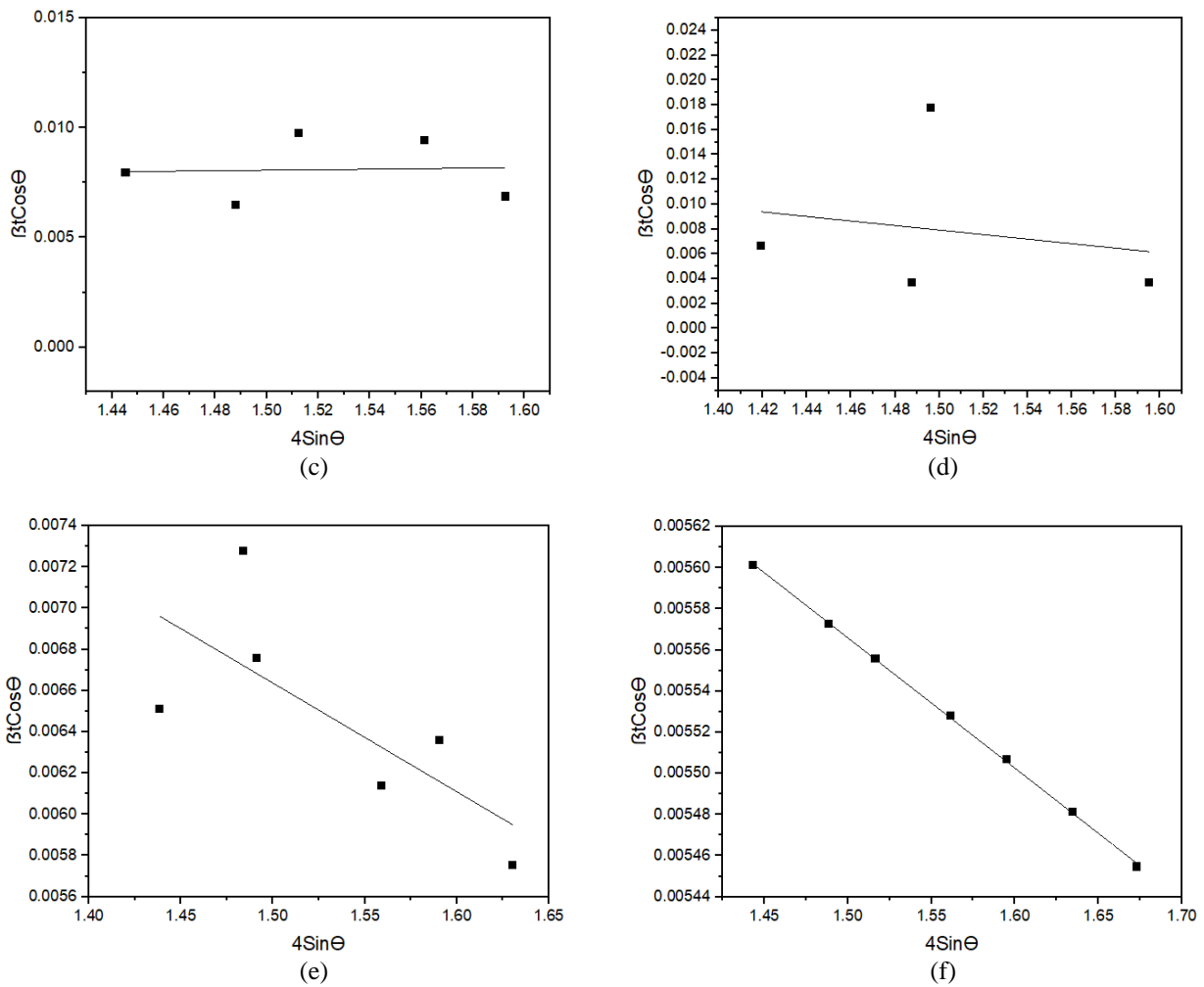


Figure 4. (cont.) (c) 2h @ 800°C ; (d) 4h @ 800°C ; (e) 8h @ 800°C ; (f) 16h @ 800°C

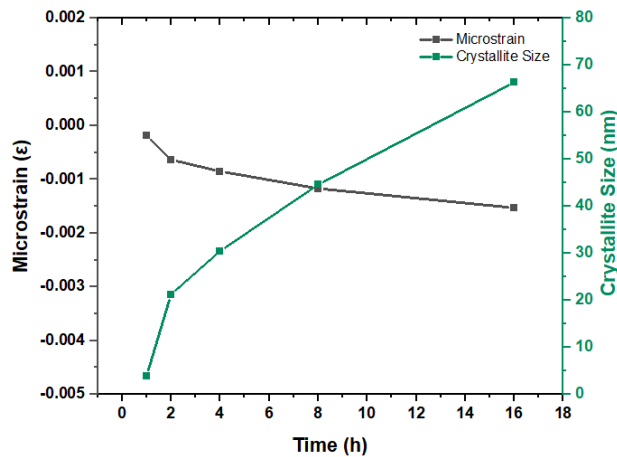


Figure 5. (a) Tetragonal sigma phase crystallite size vs exposure time (1h, 2h, 4h, 8h, and 16h) @ 800°C ; (b) microstrain in tetragonal sigma phase vs time (1h, 2h, 4h, 8h, and 16h) of exposure @ 800°C

Equimolar AlCoCrFeNi, a high entropy alloy, is amongst the most probed HEAs because of its analogy of microstructure and phase transformation with steels and titanium alloys. Unlike conventional alloy systems, it exhibited extraordinary mechanical properties with high-temperature stability and corrosion resistance. The XRD analysis in cast condition showed weak peaks corresponding to the L12 Al-Ni-phase along with B2, contrary to the finding of Zhang et al. (2022) [13] as they did not report the presence of B2 structure in cast samples. This may be due to different processing and solidification conditions. High entropy alloys have a slogan of sluggish diffusion as compared to dilute conventional alloys due to variations in atomic size and atomic percentage of alloying elements. This sluggish diffusion facilitated the restricted atomic movement of Cr (166 pm) and Fe (156 pm) because of their larger atomic radii as compared to Al (118 pm) and Ni (149 pm). The interdendritic region at the interfacial boundary was enriched with Cr and Fe contents with increased lattice parameters on rising temperature. According to recent research, the thermodynamic data suggested an

event to occur at 596.8°C, enforcing the nucleation of the FCC phase, diffusing out the Cr and Fe atoms, and diffusing in Al and Ni atoms in interdendritic regions [28]. The difference in diffusion rates between these two pairs of elements facilitated the thermodynamic and kinematic prerequisites of the tetragonal σ -phase to occur. High interfacial strain energy conferred the restricted movement of Cr and Fe atoms meeting localized co-segregation of Cr, Fe, and Co to occur [20]. The microstrain results and W-H plot slopes verified the same phenomenon. HRTEM geographical micro strain mapping validated the postulated and tetragonal structure embedded in a relatively relaxed B2 matrix and FCC neighboring crystals. The tetragonal σ -phase precipitated in stainless steels (SS) at the ferrite-austenite interface by partial breakdown of ferrite into austenite and at the border between ferrite and austenite [29, 30]. It was possible to hypothesize that under the present situation if one thinks that this system performs similarly to SS at the BCC-FCC interface, the tetragonal σ -phase will also precipitate. It was found that increasing holding time at the transformation temperature further increased the crystallite size and phase fraction of the tetragonal σ -phase, as verified by crystallite size and XRD pattern, which depicted a decrease in the intensity of BCC characteristic peaks.

However, the significant resemblance of phases in the sample quenched in water from 1250°C with the work reported by Zhao et al. (2021) and Muntiz et al. (2016) while it was contrary to the results claimed by Zhang et al. (2022) and Wang et al. (2021) [13, 31-33]. The nucleation of the intergranular FCC phase confirmed the quench sensitivity of equimolar AlCoCrFeNi HEA rather than retaining the B2/BCC phase. Their quench sensitivity refers to the ability of alloy-altering phase constituents with changing cooling rates from high homogenization of solution treatment temperatures. The precipitation of the FCC phase may contain localized nanosized co-segregation of Cr-Fe-rich clusters, stimulating curiosity about the FCC phase evolution mechanism on cooling from 1250°C. The evident binodal decomposition occurred while cooling from homogenization temperature to architect a rectilinear woven network of interlaminated Cr-Fe and Al-Ni rich alternates in the dendritic region [9, 32-34]. Such phenomenon of the irreversibility of tetragonal σ -phase on cooling from higher temperatures contrasted with the classical understanding of tetragonal σ -phase in stainless steels and Fe-Cr-rich conventional alloys [29].

4. CONCLUSIONS

This work investigated equimolar AlCoCrFeNi HEA prepared by vacuum induction melting for under-stranding and determining the kinematics of transformation in the crystal structure. Specifically, kinematics of the tetragonal σ -phase during its evolution from cast structure to transformation temperature (800°C) with variation in holding time and at homogenization temperature (1250°C) with the varying cooling rate (water quenched and furnace cooled). The findings are distinct, as they determine the increase in crystallite size while staying in the transformation temperature, which may prolong the dissolution time of the sigma phase during homogenizing or preheating for thermomechanical processing. Secondly, the cooling rate from high temperature influences the nucleation of the FCC/L12 phase and its contents, while sigma phase recurrence is not associated with cooling. It could be concluded as the following:

- XRD results suggested BCC/B2 as the major phase, while FCC was a minor phase in cast condition.
- XRD results of samples exposed at 800°C for 1h, 2h, 4h, 8h, and 16 h exhibited evidence of tetragonal σ -phase with characteristic peaks at 42.443°, 43.848°, 44.949°, 46.183°, 47.097° and 48.457°.
- The tetragonal σ -phase crystallite size kept growing from 3.12nm to 68.37 nm.
- The tetragonal σ -phase started nucleating within 1h of exposure to 800°C and kept growing, increasing the intrinsic strain as suggested by the microstrain versus time plot.
- With increasing holding time at transformation temperature, low angle peaks at 30.9° and 35.3° appeared, verifying the presence of AlNi intermetallics.
- Cooling of equimolar AlCrCoFeNi HEA from 1250°C, either in water or in a furnace, did not facilitate the reoccurrence of the tetragonal σ -phase. However, the increased intensity of FCC peaks in furnace-cooled samples suggested the quench sensitivity of the alloy. The absence of reprecipitation of the tetragonal sigma (σ) phase knocked its ability to undergo bulk thermomechanical processing for engineering applications.

ACKNOWLEDGEMENTS

This work is funded by the Ministry of Higher Education under the Fundamental Research Grant Scheme (FRGS), Registration Grant No: FRGS/1/2022/TK10/UTM/02/45

CONFLICT OF INTEREST

The authors declare no conflicts of interest regarding the publication of this paper.

AUTHORS CONTRIBUTION

Mudassar Hussain: (Conceptualization; Fabrication of alloy; Formal characterization and analysis; Visualisation; Drafting manuscript)

Abdillah Sani Mohd Najib: (Reviewing; Proofreading, Corrections)

Nor Akmal Binti Mohd Fadil: (Reviewing; Proofreading; Corrections; Resourcing)

Tuty Asma Binti Abu Bakar: (Technical Advisor; Reviewing; Proofreading; Corrections; Resourcing; Corresponding author)

REFERENCES

- [1] M. Tokarewicz and M. Grądzka-Dahlke, "Review of Recent Research on AlCoCrFeNi High-Entropy Alloy," *Metals*, vol. 11, no. 8, p. 1302, 2021.
- [2] H.Y. Chen, C.W. Tsai, C.C. Tung, J.W. Yeh, T.T. Shun, C.C. Yang *et al.*, "Effect of the substitution of Co by Mn in Al-Cr-Cu-Fe-Co-Ni high-entropy alloys," *Annales De Chimie-Science Des Materiaux*, vol. 31, no. 6, pp. 685-698, 2006.
- [3] B. Cantor, I. T. H. Chang, P. Knight, and A. J. B. Vincent, "Microstructural development in equiatomic multicomponent alloys," *Materials Science and Engineering: A*, vol. 375-377, pp. 213-218, 2004.
- [4] J.W. Yeh, S.K. Chen, S.J. Lin, J.Y. Gan, T.S. Chin, T.T. Shun *et al.*, "Nanostructured high-entropy alloys with multiple principal elements: novel alloy design concepts and outcomes," *Advanced engineering materials*, vol. 6, no. 5, pp. 299-303, 2004.
- [5] N.F. Lone, F. Czerwinski, and D. Chen, "Present challenges in development of lightweight high entropy alloys: A review," *Applied Materials Today*, vol. 39, p. 102296, 2024.
- [6] J.-W. Yeh, "Alloy design strategies and future trends in high-entropy alloys," *Journal of The Minerals, Metals & Materials Society*, vol. 65, no. 12, pp. 1759-1771, 2013.
- [7] G. Shang, L. Jiang, Z.-Z. Liu, and X.-G. Lu, "High-throughput experimental study on the microstructural and compositional variations of mechanical properties for AlCoCrFeNi high entropy alloys," *Journal of Alloys and Compounds*, vol. 917, p.165513, 2022.
- [8] S. Uporov, V. Bykov, S. Pryanichnikov, A. Shubin, and N. Uporova, "Effect of synthesis route on structure and properties of AlCoCrFeNi high-entropy alloy," *Intermetallics*, vol. 83, pp. 1-8, 2017.
- [9] C. Zhao, J. Li, Y. Liu, X. Ma, Y. Jin, W. Y. Wang *et al.*, "Optimizing mechanical and magnetic properties of AlCoCrFeNi high-entropy alloy via FCC to BCC phase transformation," *Journal of Materials Science & Technology*, vol. 86, pp. 117-126, 2021.
- [10] S. Mohanty, T. Maity, S. Mukhopadhyay, S. Sarkar, N. Gurao, S. Bhowmick *et al.*, "Powder metallurgical processing of equiatomic AlCoCrFeNi high entropy alloy: Microstructure and mechanical properties," *Materials Science and Engineering: A*, vol. 679, pp. 299-313, 2017.
- [11] W. Ji, Z. Fu, W. Wang, H. Wang, J. Zhang, Y. Wang *et al.*, "Mechanical alloying synthesis and spark plasma sintering consolidation of CoCrFeNiAl high-entropy alloy," *J Alloy Compd*, vol. 589, pp. 61-66, 2014.
- [12] E. Strumza, V. Ezersky, E. Brosh, M. Aizenshtein, and S. Hayun, "A comprehensive study of phase transitions in Al_{0.5}CoCrFeNi high-entropy alloy at intermediate temperatures (400 ≤ T ≤ 900° C)," *Journal of Alloys and Compounds*, vol. 898, p. 162955, 2022.
- [13] X. Zhang, L. Liu, K. Yao, K. Duan, F. Wu, R. Zhao *et al.*, "The phase composition characteristics of AlCoCrFeNi high entropy alloy heat-treated by simple normalizing treatment and its effects on mechanical properties," *Journal of Alloys and Compounds*, vol. 926, p. 166896, 2022.
- [14] G. Shang, Z.-z. Liu, J. Fan, and X.-G. Lu, "Effect of heat treatment on the microstructure and nanoindentation behavior of AlCoCrFeNi high entropy alloy," *Intermetallics*, vol. 169, p. 108302, 2024.
- [15] J.P. Panda, P. Arya, K. Guruvadyathri, Ravikiran, and B. S. Murty, "Studies on kinetics of BCC to FCC phase transformation in AlCoCrFeNi equiatomic high entropy alloy," *Metallurgical and Materials Transactions A*, vol. 52, no. 5, pp. 1679-1688, 2021.
- [16] M.K. Alam, M.S. Hossain, N.M. Bahadur, and S. Ahmed, "A comparative study in estimating of crystallite sizes of synthesized and natural hydroxyapatites using Scherrer Method, Williamson-Hall model, Size-Strain Plot and Halder-Wagner Method," *Journal of Molecular Structure*, vol. 1306, p. 137820, 2024.
- [17] A.S. Rogachev, D.Y. Kovalev, N.A. Kochetov, A.S. Shchukin, and S.G. Vadchenko, "Evolution of crystal structure in high-entropy AlCoCrFeNi alloy: An in situ high-temperature X-ray diffraction study," *Journal of Alloys and Compounds*, vol. 861, p. 158562, 2021.
- [18] P. Martin, C. E. Madrid-Cortes, C. Cáceres, N. Araya, C. Aguilar, and J. Cabrera, "HEAPS: A user-friendly tool for the design and exploration of high-entropy alloys based on semi-empirical parameters," *Computer Physics Communications*, vol. 278, p. 108398, 2022.
- [19] Y. Zeng, M. Man, K. Bai, and Y.-W. Zhang, "Revealing high-fidelity phase selection rules for high entropy alloys: A combined CALPHAD and machine learning study," *Materials & Design*, vol. 202, p. 109532, 2021.
- [20] L. Meshi, Y. Linden, A. Munitz, S. Salhov, and M. Pinkas, "Retardation of the σ phase formation in the AlCoCrFeNi multi-component alloy," *Materials Characterization*, vol. 148, pp. 171-177, 2019.
- [21] V. Shivam, J. Basu, V. K. Pandey, Y. Shadangi, and N. Mukhopadhyay, "Alloying behaviour, thermal stability and phase evolution in quinary AlCoCrFeNi high entropy alloy," *Advanced Powder Technology*, vol. 29, no. 9, pp. 2221-2230, 2018.
- [22] J. Menghani, A. Vyas, P. Patel, H. Natu, and S. More, "Wear, erosion and corrosion behavior of laser cladded high entropy alloy coatings – A review," *Materials Today: Proceedings*, vol. 38, pp. 2824-2829, 2021.

- [23] K. Jasiewicz, J. Cieslak, S. Kaprzyk, and J. Tobola, "Relative crystal stability of Al_xFeNiCrCo high entropy alloys from XRD analysis and formation energy calculation," *Journal of Alloys and Compounds*, vol. 648, pp. 307-312, 2015.
- [24] S.P. Zhao, Z.D. Feng, L.X. Li, X.J. Zhao, L. Lu, S. Chen *et al.*, "Dynamic mechanical properties, deformation and damage mechanisms of eutectic high-entropy alloy AlCoCrFeNi_{2.1} under plate impact," *Journal of Materials Science & Technology*, vol. 134, pp. 178-188, 2023.
- [25] Y. Li, W. Chen, C. Lu, H. Li, W. Zheng, Y. Ma *et al.*, "Microstructural evolution mediated creep deformation mechanism for the AlCoCrFeNi_{2.1} eutectic high-entropy alloy under different testing conditions," *Materials Science and Engineering: A*, vol. 857, p. 144100, 2022.
- [26] Y.L. Zhao, T. Yang, Y.R. Li, L. Fan, B. Han, Z.B. Jiao *et al.*, "Superior high-temperature properties and deformation-induced planar faults in a novel L12-strengthened high-entropy alloy," *Acta Materialia*, vol. 188, pp. 517-527, 2020.
- [27] S.W. Wu, G. Wang, J. Yi, Y.D. Jia, I. Hussain, Q.J. Zhai *et al.*, "Strong grain-size effect on deformation twinning of an Al_{0.1}CoCrFeNi high-entropy alloy," *Materials Research Letters*, vol. 5, no. 4, pp. 276-283, 2016.
- [28] E. Strumza and S. Hayun, "Comprehensive study of phase transitions in equiatomic AlCoCrFeNi high-entropy alloy," *Journal of Alloys and Compounds*, vol. 856, p. 158-220, 2021.
- [29] R. Magnabosco, "Kinetics of sigma phase formation in a duplex stainless steel," *Materials Research*, vol. 12, pp. 321-327, 2009.
- [30] C.-C. Hsieh and W. Wu, "Overview of intermetallic sigma (σ) phase precipitation in stainless steels," *International Scholarly Research Notices*, vol. 2012, p. 732471, 2012.
- [31] C. Zhao, J. Li, Y. Liu, W.Y. Wang, H. Kou, E. Beaugnon *et al.*, "Tailoring mechanical and magnetic properties of AlCoCrFeNi high-entropy alloy via phase transformation," *Journal of Materials Science & Technology*, vol. 73, pp. 83-90, 2021.
- [32] A. Munitz, S. Salhov, S. Hayun, and N. Frage, "Heat treatment impacts the micro-structure and mechanical properties of AlCoCrFeNi high entropy alloy," *Journal of Alloys and Compounds*, vol. 683, pp. 221-230, 2016.
- [33] C.T. Wang, Y. He, Z. Guo, X. Huang, Y. Chen, H. Zhang *et al.*, "Strain Rate Effects on the Mechanical Properties of an AlCoCrFeNi High-Entropy Alloy," *Metals and Materials International*, vol. 27, no. 7, pp. 2310-2318, 2021.
- [34] C. Zhao, J. Li, Y. He, J. Wang, W.Y. Wang, H. Kou *et al.*, "Effect of strong magnetic field on the microstructure and mechanical-magnetic properties of AlCoCrFeNi high-entropy alloy," *Journal of Alloys and Compounds*, vol. 820, p. 153407, 2020.